Mobility of icy sand packs, with application to Martian permafrost

William B. Durham,[1] Asmin V. Pathare,[2] Laura A. Stern,[3] and Hendrik J. Lenferink[1]

Received 4 August 2009; revised 1 October 2009; accepted 13 October 2009; published 8 December 2009.

[1] The physical state of water on Mars has fundamental ramifications for both climatology and astrobiology. The widespread presence of "softened" Martian landforms (such as impact craters) can be attributed to viscous creep of subsurface ground ice. We present laboratory experiments designed to determine the minimum amount of ice necessary to mobilize topography within Martian permafrost. Our results show that the jammed-to-mobile transition of icy sand packs neither occurs at fixed ice content nor is dependent on temperature or stress, but instead correlates strongly with the maximum dry packing density of the sand component. Viscosity also changes rapidly near the mobility transition. The results suggest a potentially lower minimum volatile inventory for the impact-pulverized megaregolith of Mars. Furthermore, the long-term preservation of partially relaxed craters implies that the ice content of Martian permafrost has remained close to that at the mobility transition throughout Martian history. **Citation:** Durham, W. B., A. V. Pathare, L. A. Stern, and H. J. Lenferink (2009), Mobility of icy sand packs, with application to Martian permafrost, *Geophys. Res. Lett.*, *36*, L23203, doi:10.1029/2009GL040392.

1. Introduction and Background

[2] Mars exhibits a wide variety of landforms that are indicative of flow, ranging from the viscous creep of ice-rich permafrost [*Squyres*, 1989; *Squyres and Carr*, 1986] to the surface mobility of thin debris flows [*Christensen*, 2003; *Milliken et al.*, 2003]. Such flow features probably contain significant amounts of dust, which for example will likely be present throughout the impact-disrupted subsurface megaregolith [*Clifford*, 1993] and inside sublimation lag layers atop ablating near-surface ice [*Hofstadter and Murray*, 1990].

[3] How much subsurface ice is implied by these observations? *Jankowski and Squyres* [1992] performed finite element simulations of crater relaxation in Martian permafrost, and concluded that at least the upper 1 km of the high-latitude subsurface must be "ice-rich." Based on laboratory experiments conducted at 263 K, *Mangold et al.* [2002] concluded that the brittle-ductile transition in ice-rock mixtures occurs at an ice fraction of about 0.28, which they argued must be the *minimum* water ice content at a depth of 1 km to initiate surface relaxation. Assuming an exponential porosity decay constant of 2.82 km [*Clifford*, 1993], this implies a columnar ice content of 34% in the upper km (at all latitudes poleward of 30°), corresponding to at least 200 global meters of water [*Mangold et al.*, 2002]. However, we have previously demonstrated the importance of performing deformation experiments involving ice at colder temperatures more relevant to planetary conditions [*Durham et al.*, 1992], thus providing the motivation for the current study.

[4] Here, we present results from a series of laboratory creep experiments aimed at finding the minimum amount of ice necessary to mobilize topography within Martian permafrost. Absent tectonic forces and significant horizontal density contrasts, subsurface viscous deformation is driven by shear stresses on the order of overburden pressure times the sine of the surface slope [*Paterson*, 1994]. Normal stresses on Mars therefore generally greatly exceed shear stresses, which assures that landform modification takes place primarily via ductile rather than brittle deformation mechanisms. To speed up the simulated geologic time scale, we apply an exaggerated level of shear stress, along with a commensurate increase in confining pressure to suppress brittle deformation. We avoid temperatures above 250 K to prevent obfuscating rheological effects related to premelting in ice [*Dash et al.*, 1995].

[5] We previously conducted measurements of the rheological properties of ice-rich mixtures ranging from 42% to 100% ice by volume [*Durham et al.*, 1992]. Recent studies have explored the brittle-to-ductile transition of sand-rich mixtures, with application to very near-surface planetary features [*Mangold et al.*, 2002; *Yasui and Arakawa*, 2008]. The present study, however, represents the first comprehensive mapping of the boundary between ductility and complete immobility in sand/ice mixtures at conditions relevant to planetary settings.

2. Rheology of Icy Sand Packs at Planetary Conditions

[6] We characterize sample composition here by the relative volume fractions of sand, f, and triple-distilled water ice, $1 - f$, leaving unspecified the small volume fraction of air-filled porosity vented to atmosphere. Samples were always tested under confining pressures $\geq$60 MPa, so open porosity existed only where pores could be bridged by sand grains—in other words, only in undersaturated, ice-poor samples. We tested frozen sand packs of two different sand bases designed to give a wide range of sand packing densities: pure Oklahoma #1 (OK #1), and a 2:1 by volume mixture of Flint Silica #12 and OK #1. Both sands are high-purity quartz sands with trace amounts of hematite, illite, calcite, and alumina. OK #1 has a narrow distribution of grain size, with 84% of the grains having a diameter between 0.106 and 0.25 mm. The grain size range of Flint #12 is approximately 1–2 mm. The porosity of OK #1 loosely poured is 0.42 ± 0.02; with shaking, porosity can be reduced to 0.32 ± 0.02. This compares reasonably to

[1]Department of Earth, Atmospheric, and Planetary Sciences, Massachusetts Institute of Technology, Cambridge, Massachusetts, USA.
[2]Planetary Science Institute, Pasadena, California, USA.
[3]U.S. Geological Survey, Menlo Park, California, USA.

0094-8276/09/2009GL040392

Table 1. Experimental Conditions and Results[a]

Run (Step)	Sand	f	P, MPa	T, K	σ, MPa	$\dot{\varepsilon}_{ss}$, s^{-1} Meas	$\dot{\varepsilon}_{ss}$, s^{-1} at Std Conds[b]	ε at 10^6 s[c]
536(1)	OK #1	0.60	100	243	33	7.0×10^{-7}	3.3×10^{-8}	0.10
(2)			100	223	33	6.9×10^{-8}	4.7×10^{-8}	
(3)			60	243	32	9.5×10^{-7}	5.0×10^{-8}	
540(1)	OK #1	0.68	60	243	31			0.046
544(1)	OK #1	0.50	100	243	11	4.4×10^{-6}	1.7×10^{-5}[d]	14
(2)			100	243	23	1.2×10^{-4}	1.9×10^{-5}[d]	
(3)			100	223	20	1.2×10^{-6}	6.1×10^{-6}[d]	
(4)			100	223	28	8.6×10^{-6}	1.1×10^{-5}[d]	
546(1)	OK #1	0.68	60	223	32			0.045
549(1)	OK #1	0.90	60	223	34			0.043
550(1)	OK #1	1.00	60	223	32			0.031
551(1)	OK #1	0.80	60	223	30			0.040
552(1)	OK #1	0.64	60	223	20			(not $\dot{\varepsilon}_{ss}$)
(2)			60	223	31			(not $\dot{\varepsilon}_{ss}$)
(3)			200	223	31	3.4×10^{-8}	3.0×10^{-8}	0.035
(4)			200	223	53	2.1×10^{-7}	2.1×10^{-8}	
(5)			60	223	33	3.2×10^{-8}	2.2×10^{-8}	
553(1)	OK #1	1.00	60	223	31			0.045
565(1)	2:1 mix	0.705	60	243	31	$0.02-2 \times 10^{-5}$		0.16
(2)			60	243	27	$0.2-1.6 \times 10^{-6}$		
(3)			60	243	32	1.2×10^{-6}	6.3×10^{-8}	
566(1)	2:1 mix	0.748	60	223	31			0.049
567(1)	2:1 mix	0.739	60	223	31	$>2.3 \times 10^{-8}$[e]	$>2.1 \times 10^{-8}$[e]	0.032
(2)			60	243	26	$>3.1 \times 10^{-8}$[e]	$>4.4 \times 10^{-9}$[e]	
(3)			60	243	31	5.0×10^{-8}	3.5×10^{-9}	
569(1)	2:1 mix	0.713	60	223	31			0.037
573(1)	2:1 mix	0.708	60	223	30	1.5×10^{-8}	1.5×10^{-8}	0.076
(2)			100	223	51	8.9×10^{-8}	1.1×10^{-8}	

[a]See Table S1 for tabulation of uncertainties.
[b]Extrapolated to standard conditions (T, P, σ) = (223 K, 100 MPa, 30 MPa) using $\dot{\varepsilon}_{ss} \propto \sigma^n e^{-Q/RT}$, $n = 4$, $Q = 61$ kJ/mol, R = 8.31 J/mol · K [*Durham et al.*, 1992].
[c]Non-mobile samples: as measured; mobile samples: extrapolated based on estimated transient strain + $10^6 \cdot \dot{\varepsilon}_{ss}$ at std conds (details in Table S1).
[d]Pressure extrapolation by a factor of $e^{-(P-60\ \mathrm{MPa})V^*/RT}$, $V^* = -13 \times 10^{-6}$ m^3/mol.
[e]Final strain rate not steady-state; values are therefore upper bounds.

values for random loose and random close packing of spheres of identical size, 0.44 and 0.36, respectively [*Onoda and Liniger*, 1990], with the sub-equant shape of the OK #1 grains allowing slightly higher volume filling. The mixed sand will pack to a higher density; by trial and error we found a minimum porosity of 0.25 at the 2:1 ratio.

[7] Cylindrical samples approximately 60 mm long were molded in rigid tubes with inner diameter 2.54 mm. Fabrication was by one of three methods: for $f = 0.50$, sand and ice I granules of diameter approximately 0.20 mm were physically mixed in a cold glove box and then compacted to zero unfilled porosity at 100 MPa gas pressure. For $0.60 \leq f \leq 0.75$, sand was poured into liquid water and shaken as necessary in the molding tubes to densify to the desired level, and the mixture then frozen. For the ice-poor $f \geq 0.80$ samples, a measured amount of liquid water and sand were loosely mixed (think sand castles), then molded and frozen. After fabrication, samples were sealed in indium tubes of 0.5-mm wall thickness, loaded into our high-pressure cryogenic creep apparatus [*Durham et al.*, 1992], pressurized with N_2 gas as the confining medium, and deformed axially in compression at constant differential stress (creep).

[8] Fourteen deformation experiments were conducted at temperatures T = 223 or 243 K, confining pressure P of 60, 100, or 200 MPa, and differential stress $\sigma \approx 30$ MPa (Table 1). Sample compositions ranged from $0.50 \leq f \leq 1.00$. Resultant strain rates were typically low, and experiments often lasted a week or more. Two experimental run records are shown in Figure 1. All runs displayed an initial transient strain hardening followed by creep that approached a terminal "steady-state" rate, $\dot{\varepsilon}_{ss}$, in a manner common to many metals, ceramics, and other geologic materials [*Poirier*, 1985]. In the case of the most ice-poor samples, the terminal strain rate appeared to be zero (resolution limit $\sim 3 \times 10^{-9}$ s^{-1}), the sand pack becoming jammed and no longer deformable (Table 1). The state of permanent deformability, which we term mobility to contrast with the jammed state, appeared at ice fractions slightly above saturation. We focus here on the location and mechanism of the mobility transition.

[9] Mobility is depicted as a function of f in Figure 2, where the vertical axis, strain after 10^6 s under load (ε at 10^6 s) is the limiting strain for sand packs that become jammed, and is inversely related to viscosity for sand packs that are mobile. Ice-poor samples, i.e., those for which f exceeds that at maximum dry packing density, show a limiting strain near 0.04 ± 0.02 with no clear dependence on ice content or, for that matter, upon sand base. However, the location in f space of the transition to mobility clearly changes with sand base, as dramatically demonstrated by Figure 1, where the $f = 0.705$ mixed sand is mobile while the more ice-rich $f = 0.68$ OK#1 sample is jammed. For the 2:1 mixed sand (maximum dry packing 0.75) the transition is at $f = 0.710 \pm 0.015$, while for the pure OK#1 sand (maximum dry packing 0.68) the transition is at $f = 0.62 \pm 0.03$ (Figure 2, shaded zones).

[10] Relative viscosity rapidly escalates in the vicinity of the mobility boundary. Whereas viscosity in the interval $0 \leq f \leq 0.58$ (dashed line in Figure 2 inset) is linear in log space and gradual, spanning approximately two orders of magni-

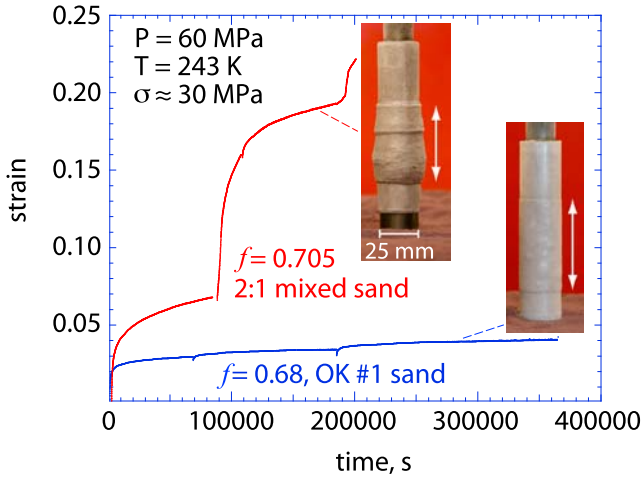

Figure 1. Strain-time records illustrating the effect of sand base. Photographs of respective samples show sample assembly, including top and bottom deformation pistons and sample (arrow tip to arrow tip), encapsulated in a pressure-sealed 0.5-mm thick indium jacket. At nearly identical test conditions, the sample with higher ice content, f = 0.68 (Run 540; also shown in Figure S1c), strain hardened to a jammed state by strain 0.04, while the sample with the lower ice content, f = 0.705 (Run 565; also shown in Figures S1e and S1f), deformed without limit. The most important difference between the samples is the sand base, the former being pure OK #1 sand and the latter the 2:1 Flint Silica #12:OK #1 sand mix. Distinctly nonuniform strain in the f = 0.705 sample indicated by its irregular profile, as well as a sharp increase in strain rate at 90000 s and subsequent return to lower rate, represents actual extreme spatial and temporal variations in viscosity. We associate these with sensitivity of viscosity to f near the mobility transition. The ridge in the upper third of the f = 0.705 sample is an ice-rich joint introduced during sample preparation before deformation, where a 10-mm disc was removed for CSEM analysis (Figure S1e). A similar variation in strain was seen in sample 573 (f = 0.708), also a 2:1 mix, which exhibited a less pronounced tapered shape because total strain was lower. Local strain varied by roughly a factor of 5, increasing monotonically from top to bottom. Subtle variations in f within any sample would not be unexpected (Figure S1), and where rheological behavior is extremely sensitive to f, pronounced nonuniformities in strain rate might result.

tude [*Durham et al.*, 1992], at $f > 0.58$ viscosity increases by at least another two orders of magnitude over a fairly small interval of f (dot-dashed lines in Figure 2 inset). Mobile sand packs exhibit characteristics of ice I rheology: several sets of intra-run comparative measurements in which conditions were varied (Runs 536, 544, 552, and 573) qualitatively reproduce the pronounced σ and T dependence of steady-state flow of ice I (Table 1). Conversely, ε at 10^6 s on the jammed side shows no T effect between 243 and 223 K in the one instance where comparison is possible (Runs 540 versus 546, Table 1).

[11] The structure of the deformed samples provides additional clues as to the nature of the unjamming mechanism. Ice-poor material contains broken and crushed sand grains, with the amount of fractured sand decreasing steadily with increasing ice content up to saturation. Evidently the presence of ice slightly in excess of saturation suppresses fracture at the grain contacts, either by providing increased confinement [*Jaeger and Cook*, 1976] or by bearing some of the applied load itself and thereby reducing the normal stress at grain contacts. In the former case the mobile state suggests that ice must act to lubricate sand grain-grain contacts. In the latter scenario, the ice itself must experience finite deviatoric stress; deformation will then necessarily continue as long as load is applied, and will be limited by the viscosity of ice. Further details of sample structure, including cryogenic scanning electron microscope images, can be found in the auxiliary materials, Figure S1.[1]

3. Jammed-to-Mobile Transition

[12] The fact that mobile samples in this study do exhibit the T and σ dependence of pure ice I supports the second mechanism, that the normal stress at sand grain contacts is reduced due to ice bearing some of the applied load, but does not explain how a sand pack transforms from jammed to mobile with the addition of only a slight amount of ice. Parallels to this behavior exist in certain jammed granular systems that are referred to as "fragile matter" [*Cates et al.*, 1998]. Rigid support in these systems exists through "force chains" of contacting particles, and an infinitesimal change in deviatoric stress orientation can cause very large inelastic reorganizations of grains [*Cates et al.*, 1998]. Minute changes to other factors such as packing fraction and even T can have the same effect [*Howell et al.*, 1999; *Liu and Nagel*, 1998]. Examples of fragile behavior in granular systems abound, from avalanches to glass transitions to frictional sliding [e.g., *Liu and Nagel*, 1998; *Mehta*, 2007].

[13] The picture emerges in our samples of a viscous avalanche [*Courrech du Pont et al.*, 2003]. At a critical value of ice oversaturation, ~0.05 volume fraction ice above that at maximum sand packing, the existence of finite deviatoric stress in the ice component allows sufficient elastic and plastic displacement that some force chain will always fail, preventing permanent jamming and continually triggering avalanche behavior. Beyond critical saturation the motion is continuous, and by analogy to granular flow in a fluid medium [*Courrech du Pont et al.*, 2003], sand motion then proceeds at a rate that is controlled by the viscosity of the ice component. The instability implied by the avalanche scenario may help explain anomalous behavior of two mobile sand packs close to the transition composition (see Figure 1 caption).

[14] Our results provide significant new constraint regarding the rheology of mobile sand-ice mixtures at high sand fractions. Our previous measurements reached approximately f = 0.58, where we observed a relative viscosity with respect to pure ice (f = 0) of 10^2 [*Durham et al.*, 1992]; here, we measure a relative viscosity near the mobility boundary on the order of 10^4 (Figure 2). Given that the minimum observable strain rate on the time scale of our laboratory experiments is 3×10^{-9} s^{-1}, the highest

[1] Auxiliary materials are available in the HTML. doi:10.1029/2009GL040392.

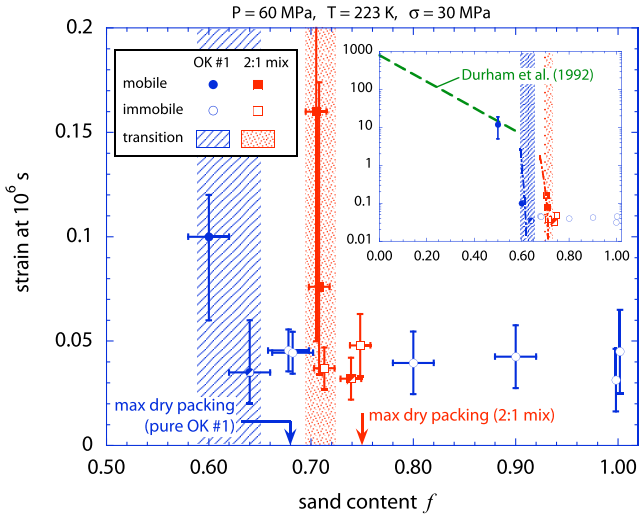

Figure 2. Transition of frozen sand packs from jammed to mobile as a function of sand content for sand + ice samples of two different sand bases, pure OK #1 (circles) and the 2:1 mix (squares). Values are extrapolated to the indicated common conditions of T, P, and σ for purposes of graphical comparison (see Table 1 for details). Open porosity, i.e., non ice-filled, exists only to the right of the arrows indicating "max dry packing" for the respective sand bases. Solid symbols indicate mobility, i.e., $\dot{\varepsilon}_{ss} > 0$ in Table 1; open symbols indicate an end state that is jammed. Two samples exhibited mixed behavior. Where run time did not reach 10^6 s, values were extrapolated (see Table S1). To the left of the transition (the shaded vertical zones), the ordinate may be read as an inverse viscosity. The dashed curve in the inset is relative viscosity for OK#1 sand + ice [*Durham et al.*, 1992]. Dot-dashed curves are interpolated trends of inverse viscosities for the two sand bases. Note that the ordinate on the inset is a log scale. Error bars are explained in Table S1. The large vertical error bars of the two solid squares in the main figure indicate temporal and spatial variation of strain rate in those samples (see text).

viscosity contrast we can resolve in the units of Figure 2 is $(10^6 \cdot 3 \times 10^{-9}) = 0.003$, or a relative viscosity of roughly $10^{4.5}$ with respect to pure ice. Over the much longer time scale of Martian geology, relative viscosity near the transition could be substantially higher than $10^{4.5}$. Additionally, the trend of relative viscosity versus f is not necessarily vertical at the lab observation limit (dot-dashed curves in Figure 2 inset), so the transition may occur at a slightly higher value of f. Under the viscous avalanche mechanism, an upper bound for f must be the dry packing limit, since at that point essentially all sand grains belong to force chains. More precise speculation about the planetary f at transition is difficult.

4. Implications for the Evolution of the Martian Cryosphere

[15] By the end of the Late Heavy Bombardment (~3.9 Ga), intense impact cratering would have produced a loosely agglomerated megaregolith that was several kilometers thick [*Clifford*, 1993]. As global temperatures cooled later in the Noachian, liquid water would begin to freeze downward from the surface, resulting in the formation of a saturated, ice-rich permafrost zone above a submerged hydrosphere, which is consistent with observations of catastrophic flood channel outbursts throughout the Hesperian [*Baker et al.*, 1992]. To the extent that the behavior shown in Figure 2, that of a frozen sand pack of rounded, non-cemented granules, applies to the near surface of Mars, we can speculate about the behavior of a cryosphere that is mobile and potentially many orders of magnitude more viscous than pure ice.

[16] By not tying viscosity to a fixed ice content, but rather to the packing characteristics of the particular granular material that is present, one may assert that any granular mix can find any viscosity. The rapid increase in viscosity near the mobility transition can explain the widespread distribution of softened craters on the Martian surface, the continued presence of which is problematic given that calculated crater relaxation times at mid- and high latitudes are millions of years or less. *Turtle and Pathare* [2005] modeled the "softening" of mid-latitude Martian craters in ice-rich permafrost, and even when using relative viscosities ~100 times greater than pure ice (in accordance with the maximum values measured by *Durham et al.* [1992] plotted along the green line in Figure 2), calculated that D = 3 km craters should relax on time scales of at most millions of years. However, our current results indicate that viscosity increases can far exceed a factor of 100 (Figure 2). Hence, the paradoxical persistence of partially relaxed craters for billions of years can be resolved if subsurface ice content has always remained near the high-viscosity mobility transition. Making the plausible assumption that the cryosphere was oversaturated by only a very small amount in the late Noachian and stayed in this slightly oversaturated state for an extended period of Martian history, it becomes possible to explain incomplete landform softening without requiring a serendipitous ice content and an unrealistically brief period of ice saturation [*Turtle and Pathare*, 2005].

[17] The depth dependence of porosity has important ramifications for the total thickness of the mobile Martian permafrost layer. Previous workers have assumed exponentially decaying porosity with depth in the megaregolith [*Clifford*, 1993; *Mangold et al.*, 2002]; however, ice saturation may prevent gravitational compaction, resulting in nearly constant porosity with depth. If porosity does decay exponentially, there should be a "critical depth" corresponding to the ice content of the mobility transition below which the subsurface is no longer capable of ductility (approximately 1 km, according to *Jankowski and Squyres* [1993] and *Mangold et al.* [2002]). Since any crater that penetrates the critical depth will not exhibit the same pattern of topographic relaxation seen in shallower crater cavities, one clear test of the porosity profile would be to model the effects of deformation layer thickness upon the observed diameter-dependence of crater relaxation. Although such a study has not yet been systematically performed, we note that softened diameter $D \approx 40$ km craters have been observed in numerous Viking images [*Jankowski and Squyres*, 1992; *Squyres*, 1989]. According to MOLA-derived empirical relationships [*Garvin et al.*, 2002], fresh $D = 40$ km Martian craters will have average depths of

2.2 km and average rim heights of 460 m, which means that they typically penetrate to a depth of 1.7 km beneath the pre-impact surface. Thus the widespread presence of such large terrain-softened Martian craters [*Jankowski and Squyres*, 1992; *Squyres*, 1989; *Squyres and Carr*, 1986] is more consistent with near-constant porosity than with exponentially decaying porosities at these depths.

[18] Our laboratory results indicate that the mobility transition does not occur at fixed ice content, but instead varies with the maximum sand packing density. Although it is obviously difficult to determine this maximum packing fraction (f_{max}) for the Martian subsurface *a priori*, we can assume it lies somewhere between the value of 0.36 corresponding to random close packing of perfect spheres [*Onoda and Liniger*, 1990] and the low lunar surface porosity of 0.20 [*Clifford*, 1993]. Accounting for a maximum oversaturation of 0.05, the *f*-space offset between the mobility transition and maximum dry packing (Figure 2), then following *Mangold et al.* [2002], we calculate that the ice content of the upper 1 km of Mars must range between 210–240 global meters of water (for $f_{max} = 0.36$) and 120–150 global meters of water (for $f_{max} = 0.20$). In contrast, the *Mangold et al.* [2002] estimate of 200 m is merely a lower limit. Therefore, for a given sand base our results more tightly constrain the ice content of the Martian cryosphere throughout its geologic history.

[19] **Acknowledgments.** The authors gratefully acknowledge support by NASA Mars Fundamental Research grant NNX08AT14G. HJL acknowledges support from the MIT Grayce B. Kerr Fellowship.

References

Baker, V. R., M. H. Carr, V. C. Gulick, C. R. Williams, and M. S. Marley (1992), Channels and Valley Networks, in *Mars*, edited by H. H. Kieffer et al., pp. 493–522, Univ. of Ariz. Press, Tucson.

Cates, M. E., J. P. Wittmer, J. P. Bouchaud, and P. Claudin (1998), Jamming, force chains, and fragile matter, *Phys. Rev. Lett.*, *81*, 1841–1844, doi:10.1103/PhysRevLett.81.1841.

Christensen, P. R. (2003), Formation of recent Martian gullies through melting of extensive water-rich snow deposits, *Nature*, *422*, 45–48, doi:10.1038/nature01436.

Clifford, S. M. (1993), A model for the hydrologic and climatic behaviour of water on Mars, *J. Geophys. Res.*, *98*, 10,973–11,016, doi:10.1029/93JE00225.

Courrech du Pont, S., P. Gondret, B. Perrin, and M. Rabaud (2003), Granular avalanches in fluids, *Phys. Rev. Lett.*, *90*, 044301, doi:10.1103/PhysRevLett.90.044301.

Dash, J. G., H. Hu, and J. S. Wettlaufer (1995), The premelting of ice and its environmental consequences, *Rep. Prog. Phys.*, *58*, 115–167, doi:10.1088/0034-4885/58/1/003.

Durham, W. B., S. H. Kirby, and L. A. Stern (1992), Effects of dispersed particulates on the rheology of water ice at planetary conditions, *J. Geophys. Res.*, *97*, 20,883–20,897, doi:10.1029/92JE02326.

Garvin, J. B., S. E. H. Sakimoto, J. J. Frawley, and C. Schnetzler (2002), Global geometric properties of Martian impact craters, *Lunar Planet. Sci. Conf.*, *XXXIII*, Abstract 1255.

Hofstadter, M. D., and B. C. Murray (1990), Ice sublimation and rheology: implications for the Martian polar layered deposits, *Icarus*, *84*, 352–361, doi:10.1016/0019-1035(90)90043-9.

Howell, D., R. P. Behringer, and C. Veje (1999), Stress fluctuations in a 2D granular Couette experiment: A continuous transition, *Phys. Rev. Lett.*, *82*, 5241–5244, doi:10.1103/PhysRevLett.82.5241.

Jaeger, J. C., and N. G. W. Cook (1976), *Fundamentals of Rock Mechanics*, 2nd ed., pp. 86–94, Chapman and Hall, London.

Jankowski, D. G., and S. W. Squyres (1992), The topography of impact craters in softened terrain on Mars, *Icarus*, *100*, 26–39, doi:10.1016/0019-1035(92)90015-Y.

Jankowski, D. G., and S. W. Squyres (1993), "Softened" impact craters on Mars: Implications for ground ice and the structure of the Martian megaregolith, *Icarus*, *106*, 365–379, doi:10.1006/icar.1993.1178.

Liu, A. J., and S. R. Nagel (1998), Nonlinear dynamics: Jamming is not just cool any more, *Nature*, *396*, 21–22, doi:10.1038/23819.

Mangold, N., P. Allemand, P. Duval, Y. Geraud, and P. Thomas (2002), Experimental and theoretical deformation of ice-rock mixtures: Implications on rheology and ice content of Martian permafrost, *Planet. Space Sci.*, *50*, 385–401, doi:10.1016/S0032-0633(02)00005-3.

Mehta, A. (2007), *Granular Physics*, 305 pp., Cambridge Univ. Press, New York.

Milliken, R. E., J. F. Mustard, and D. L. Goldsby (2003), Viscous flow features on the surface of Mars: Observations from high-resolution Mars Orbiter Camera (MOC) images, *J. Geophys. Res.*, *108*(E6), 5057, doi:10.1029/2002JE002005.

Onoda, G. Y., and E. G. Liniger (1990), Random loose packings of uniform spheres and the dilatancy onset, *Phys. Rev. Lett.*, *64*, 2727–2730, doi:10.1103/PhysRevLett.64.2727.

Paterson, W. S. B. (1994), *The Physics of Glaciers*, 3rd ed., 250 pp., Pergammon, Oxford, U. K.

Poirier, J.-P. (1985), *Creep of Crystals*, 260 pp., Cambridge Univ. Press, New York.

Squyres, S. W. (1989), Urey prize lecture: Water on Mars, *Icarus*, *79*, 229–288, doi:10.1016/0019-1035(89)90078-X.

Squyres, S. W., and M. H. Carr (1986), Geomorphic evidence for the distribution of ground ice on Mars, *Science*, *231*, 249–252, doi:10.1126/science.231.4735.249.

Turtle, E. P., and A. V. Pathare (2005), "Softening" of Martian impact craters by creep of ice-rich permafrost, paper presented at Workshop on the Role of Volatiles and Atmospheres on Martian Craters, Johns Hopkins Univ. Appl. Phys. Lab., Laurel, Md.

Yasui, M., and M. Arakawa (2008), Experimental study on the rate dependent strength of ice-silica mixture with silica volume fractions up to 0.63, *Geophys. Res. Lett.*, *35*, L12206, doi:10.1029/2008GL033787.

W. B. Durham and H. J. Lenferink, Department of Earth, Atmospheric, and Planetary Sciences, Massachusetts Institute of Technology, Cambridge, MA 02139–4307, USA. (wbdurham@mit.edu)

A. V. Pathare, Planetary Science Institute, 225 S. Lake Ave., Pasadena, CA 91101–3005, USA.

L. A. Stern, U.S. Geological Survey, MS 977, Menlo Park, CA 94025, USA.